LETTER

A quantum gate between a flying optical photon and a single trapped atom

Andreas Reiserer[1], Norbert Kalb[1], Gerhard Rempe[1] & Stephan Ritter[1]

The steady increase in control over individual quantum systems supports the promotion of a quantum technology that could provide functionalities beyond those of any classical device. Two particularly promising applications have been explored during the past decade: photon-based quantum communication, which guarantees unbreakable encryption[1] but which still has to be scaled to high rates over large distances, and quantum computation, which will fundamentally enhance computability[2] if it can be scaled to a large number of quantum bits (qubits). It was realized early on that a hybrid system of light qubits and matter qubits[3] could solve the scalability problem of each field—that of communication by use of quantum repeaters[4], and that of computation by use of an optical interconnect between smaller quantum processors[5,6]. To this end, the development of a robust two-qubit gate that allows the linking of distant computational nodes is "a pressing challenge"[6]. Here we demonstrate such a quantum gate between the spin state of a single trapped atom and the polarization state of an optical photon contained in a faint laser pulse. The gate mechanism presented[7,8] is deterministic and robust, and is expected to be applicable to almost any matter qubit. It is based on reflection of the photonic qubit from a cavity that provides strong light–matter coupling. To demonstrate its versatility, we use the quantum gate to create atom–photon, atom–photon–photon and photon–photon entangled states from separable input states. We expect our experiment to enable various applications, including the generation of atomic[9] and photonic[10] cluster states and Schrödinger-cat states[11], deterministic photonic Bell-state measurements[12], scalable quantum computation[7] and quantum communication using a redundant quantum parity code[13].

Since their infancy, the fields of quantum communication and quantum computation have been largely independent. For communication[1], optical photons are used because they allow the transmission of quantum states, such as time-bin or polarization qubits, over large distances using existing telecommunication fibre technology. Quantum computation[2], on the other hand, is typically based on single spins, either in vacuum or in specific solid-state host materials. In addition to the long coherence times that these spins can exhibit, they provide deterministic interaction mechanisms that facilitate local two-qubit quantum gates. Scalability would be offered by combining the specific advantages of both information carriers—namely, spins and photons[5,6]. To implement the required interaction between the different types of qubits, a deterministic quantum gate between a photon and an atom has been proposed[7]. Here we demonstrate this quantum gate and its potential for quantum information processing with atoms and photons.

The mechanism[8] we use is based on cavity quantum electrodynamics. When a photon interacts with a cavity containing a single, resonant emitter, it experiences a phase shift[14,15] which depends on the coupling strength. In our experiment, the emitter is a single ^{87}Rb atom, which is trapped at the centre of an overcoupled cavity. Full control over the position and motion of the atom[16] puts the system into the strong-coupling regime (measured coupling constant $g = 2\pi \times 6.7$ MHz, atomic dipole decay rate $\gamma = 2\pi \times 3.0$ MHz, cavity field decay rate $\kappa = 2\pi \times 2.5$ MHz). In this regime, the conditional phase shift induced on

a reflected light field[8] is π, which is the prerequisite for the quantum gate presented in this work.

In contrast to the original proposal[7], our implementation does not require interferometric stability, as the a.c. Stark shift of a linearly polarized dipole trap is used to split the Zeeman states of the excited atomic state manifold (see Methods and the level scheme in Fig. 1a). Thus, the coupling is only strong when the atom (a) is in state $|\uparrow^a\rangle$ and photons (p) of right-circular polarization $|\uparrow^p\rangle$ are reflected (green arrow and sphere in Fig. 1a). For all other qubit combinations (red arrows and sphere), the coupling is negligible because any atomic transition is detuned (see Methods). Therefore, the reflection of a photon results in a conditional phase shift of π, that is, a sign change, between the atomic and the photonic qubit:

$$|\uparrow^a\uparrow^p\rangle \rightarrow |\uparrow^a\uparrow^p\rangle$$
$$|\downarrow^a\uparrow^p\rangle \rightarrow -|\downarrow^a\uparrow^p\rangle$$
$$|\uparrow^a\downarrow^p\rangle \rightarrow -|\uparrow^a\downarrow^p\rangle$$
$$|\downarrow^a\downarrow^p\rangle \rightarrow -|\downarrow^a\downarrow^p\rangle$$

This conditional phase shift allows the construction of a universal quantum gate that can be transformed into any two-qubit gate using rotations of the individual qubits, which are implemented with wave plates for the photon and with Raman transitions for the atom. With respect to the photonic basis states $|\uparrow_x^p\rangle \equiv \frac{1}{\sqrt{2}}(|\uparrow^p\rangle + |\downarrow^p\rangle)$ and $|\downarrow_x^p\rangle \equiv \frac{1}{\sqrt{2}}(|\uparrow^p\rangle - |\downarrow^p\rangle)$, the conditional phase shift represents an atom–photon controlled-NOT (CNOT) gate.

The action of the quantum CNOT gate is a flip of the photonic target qubit, controlled by the quantum state of the atom, similar to its classical analogue. A first step to characterize the gate is therefore to measure a classical truth table. To this end, the atomic state is prepared by optical pumping either into the uncoupled $F = 1$ states, corresponding to $|\downarrow^a\rangle$, or into the coupled $|\uparrow^a\rangle$ state (see Methods). Subsequently, faint laser pulses (average photon number $\bar{n} = 0.3$) in $|\downarrow_x^p\rangle$ or $|\uparrow_x^p\rangle$ are reflected from the cavity and measured with single-photon counting modules in a polarization-resolving set-up. To ensure spectral mode matching[7], we use a Gaussian photon wavepacket with a full-width at half-maximum (FWHM) of 0.7 µs, corresponding to a FWHM bandwidth of 0.6 MHz, which is almost an order of magnitude smaller than the cavity FWHM linewidth of 5 MHz. After the reflection process, the atomic state is measured within 3 µs using cavity-enhanced hyperfine-state detection (see Methods, Extended Data Fig. 1 and ref. 8). The results are shown in Fig. 1b (see also Extended Data Table 1a), where the bars represent the normalized probabilities of detecting a certain output state for each of the orthogonal input states.

The control and target qubits are expected to be unchanged when the control qubit is in the state $|\downarrow^a\rangle$, which is accomplished with a probability of 99%. This number is limited by imperfections in the

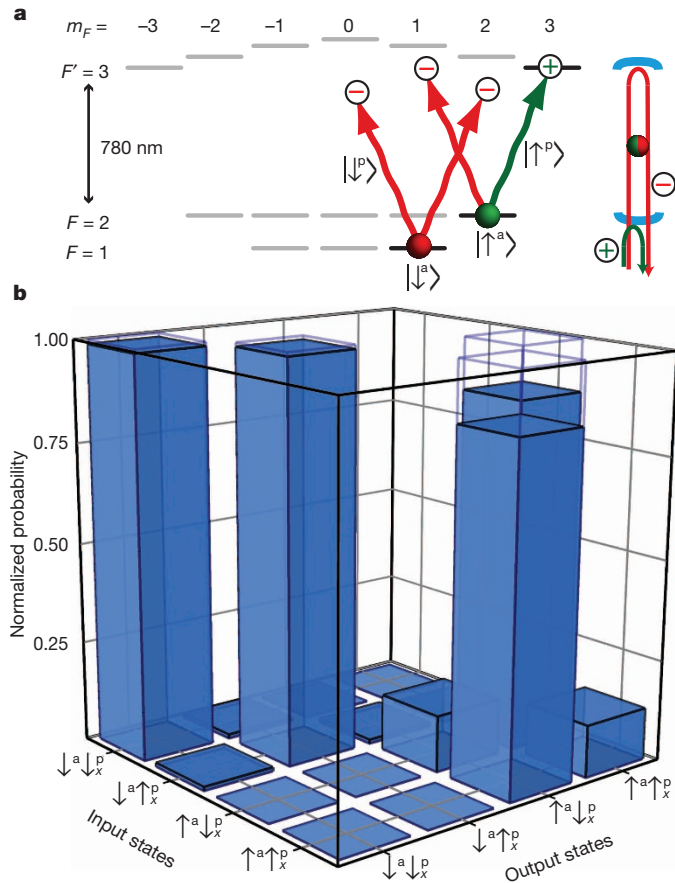[1]Max-Planck-Institut für Quantenoptik, Hans-Kopfermann-Strasse 1, 85748 Garching, Germany.

Figure 1 | Atom–photon quantum gate. a, Atomic level scheme. The photonic qubit basis states are left-circular ($|\downarrow^P\rangle$) and right-circular ($|\uparrow^P\rangle$) polarization. The atomic qubit is encoded in the $|F, m_F\rangle$ states $|\downarrow^a\rangle \equiv |1,1\rangle$ and $|\uparrow^a\rangle \equiv |2,2\rangle$. Here, F denotes the hyperfine state and m_F its projection onto an external magnetic field. The cavity (blue semicircles) is resonant with the a.c. Stark-shifted $|2,2\rangle \leftrightarrow |3,3\rangle$ transition. On reflection of a photon, the combined atom–photon state $|\uparrow^a\uparrow^P\rangle$ (green, $\oplus$) acquires a phase shift of π with respect to all other states (red, $\ominus$). **b,** Measured truth table, showing the normalized probability of obtaining a certain output state for a complete orthogonal set of input states. Open blue bars indicate an ideal CNOT gate.

detection of the photon polarization and the atomic hyperfine state. When the control qubit is in $|\uparrow^a\rangle$, the expected flip of the photonic target qubit is observed with a probability of 86%. The statistical errors in the depicted data are negligible. However, we observe ambient-temperature-related drifts of about 2% on a timescale of several hours. The flip probability is predominantly limited by three effects: first, by optical mode matching, because the transverse overlap between the free-space mode of the photon and the cavity mode is 92(3)%. Second, by the quality of preparation of the state $|\uparrow^a\rangle$, which is successful with 96(1)% probability. Last, by the stability of the difference between the cavity resonance and the frequency of the impinging laser pulse, which is about 300 kHz. None of these imperfections has a fundamental limit.

The decisive feature that distinguishes a quantum gate from a classical one is the generation of entangled states from separable input states. To characterize this property, faint laser pulses ($\bar{n} = 0.07$, FWHM 0.7 μs) are reflected from the set-up and the evaluation is post-selected on those cases where a single photon has subsequently been detected. The input state is $|\downarrow_x^a\downarrow_x^P\rangle$, such that the gate generates the maximally entangled $|\Phi_{ap}^+\rangle$ state:

$$|\downarrow_x^a\downarrow_x^P\rangle \rightarrow |\Phi_{ap}^+\rangle = \frac{1}{\sqrt{2}}\left(|\downarrow^a\downarrow_x^P\rangle + |\uparrow^a\uparrow_x^P\rangle\right)$$

Both the atomic and the photonic qubits are measured in three orthogonal bases. This allows us to reconstruct the density matrix ρ_{ap} of

the combined atom–photon state using quantum-state tomography and a maximum-likelihood estimation[17]. The result is shown in Fig. 2 (see also Extended Data Table 1b). In accordance with the truth table measurement above, the density matrix is slightly asymmetric. Whereas the value of $|\downarrow_x^a\downarrow_x^P\rangle\langle\downarrow_x^a\downarrow_x^P|$ (left corner) is close to the ideal 0.5, the elements in the other corners are smaller. The fidelity with the expected $|\Phi_{ap}^+\rangle$ state is $F_{\Phi_{ap}^+} = \langle\Phi_{ap}^+|\rho_{ap}|\Phi_{ap}^+\rangle = 80.7(0.5)\%$, where the standard error has been determined with the Monte Carlo technique[17]. In the depicted measurement, the fidelity with a slightly rotated, maximally entangled state of the form $\frac{1}{\sqrt{2}}\left(|\uparrow^a\uparrow_x^P\rangle + e^{-i\varphi}|\downarrow^a\downarrow_x^P\rangle\right)$ can be higher, probably due to a small frequency offset between the cavity and the photon. We find a maximum value of 83.0% for $\varphi = 0.11\pi$.

The major experimental imperfections that reduce the fidelity are as follows (see Methods for details): first, the above-mentioned spatial mode mismatch between cavity and impinging photon (reduction 8(3)%); second, the quality of our atomic state preparation, rotation and readout (see Extended Data Fig. 2; reduction 5(1)%); third, imperfections in the photonic polarization measurement and detector dark counts (reduction 3%); and last, the small probability of having more than one photon in the impinging laser pulses (reduction 2%). Again, none of these limitations is fundamental.

In principle, the gate mechanism presented in this work is deterministic. In our experimental implementation, the photon is not back-reflected[8] from the coupled system $|\uparrow^a\uparrow^P\rangle$ with a probability of 34(2)% (due to the finite cooperativity $C = \dfrac{g^2}{2\kappa\gamma} = 3$) and in the uncoupled cases with a probability of 30(2)% (due to the non-zero transmission of the highly reflecting cavity mirror and the mirror scattering and absorption losses, see ref. 8 and Methods). The small difference in reflectivity also contributes slightly (<1%) to the observed reduction in fidelity[9]. The achieved loss level nevertheless allows for scalable quantum computation[18] and deterministic quantum state transfer[19]. One would still observe non-classical correlations without post-selection if a perfect single-photon source and a perfect detector were used
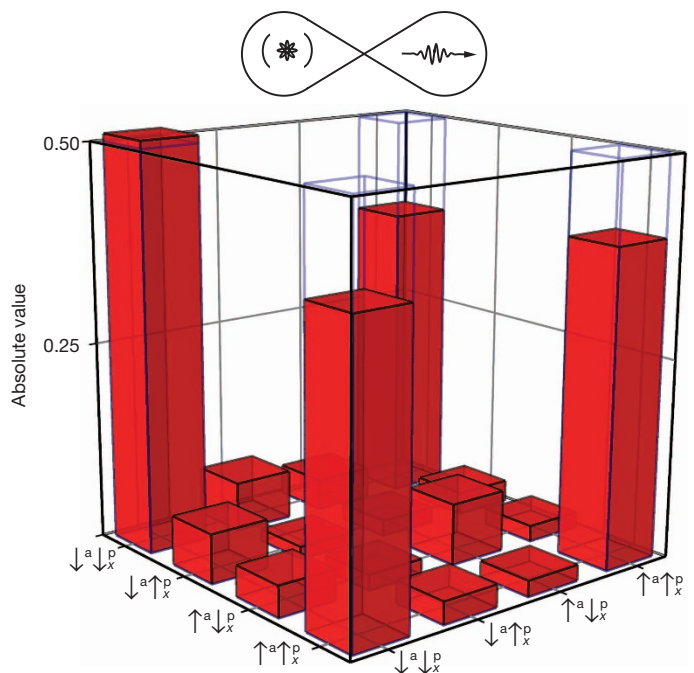

Figure 2 | Entangled atom–photon state generated via the gate operation. The bars show the absolute value of the density-matrix elements. The fidelity with the maximally entangled $|\Phi_{ap}^+\rangle$ Bell state (open blue bars) is 80.7(0.5)%. The diagram at the top of the figure symbolizes atom–photon entanglement.
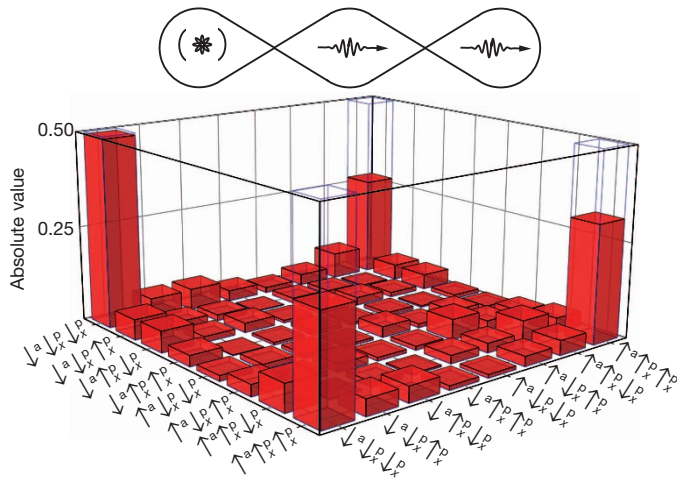
Figure 3 | Entangled state between one atom and two photons. This state is generated by reflecting two faint laser pulses from the cavity. The bars show the absolute value of the reconstructed density matrix elements. The fidelity with the maximally entangled state $|\mathrm{GHZ}\rangle$ is 61(2)%. The matrix elements of $|\mathrm{GHZ}\rangle$ are depicted as open blue bars. The diagram at the top of the figure symbolizes entanglement between an atom and two photons.

to characterize our device. We also expect that it will be possible to dramatically improve the achieved gate efficiency in next-generation cavities with increased atom–cavity coupling strength[20–23] and reduced losses.

The demonstrated quantum gate also allows the generation of entangled cluster states that consist of a trapped atom and several flying photons; this is complementary to experiments with flying atoms and trapped microwave photons[24]. To this end, the gate is applied to the photons contained in two sequentially impinging laser pulses (temporal separation 3 µs). Post-selecting events where one photon was detected in each of the input pulses, a maximally entangled Greenberger–Horne–Zeilinger (GHZ) state is expected:

$$\left|\downarrow_x^a \downarrow_x^P \downarrow_x^P\right\rangle \rightarrow |\mathrm{GHZ}\rangle = \frac{1}{\sqrt{2}}\left(\left|\uparrow^a \uparrow_x^P \uparrow_x^P\right\rangle - \left|\downarrow^a \downarrow_x^P \downarrow_x^P\right\rangle\right)$$

The density matrix of the generated quantum state, again reconstructed using quantum state tomography and a maximum-likelihood estimation, is shown in Fig. 3 (see also Extended Data Table 1c). The fidelity with the ideal state $|\mathrm{GHZ}\rangle$ (open blue bars in Fig. 3) is 61(2)%, proving genuine three-particle (atom–photon–photon) entanglement. The reasons for a non-unity fidelity are analogous to those for the case of two particles. Again, we experimentally find a higher fidelity of 67% with the slightly rotated GHZ state $\frac{1}{\sqrt{2}}\left(\left|\uparrow^a \uparrow_x^P \uparrow_x^P\right\rangle - e^{-i\varphi}\left|\downarrow^a \downarrow_x^P \downarrow_x^P\right\rangle\right)$, with $\varphi = 0.21\pi$.

Finally, we investigate whether the presented gate mechanism can mediate a photon–photon interaction for optical quantum computing[7]. We employ a quantum eraser protocol[10] which should allow us to create a maximally entangled state out of two separable input photons. To this end, the state $|\mathrm{GHZ}\rangle$ is generated as described above and a $\pi/2$ rotation is applied to the atom, which transforms the state to:

$$\frac{1}{\sqrt{2}}\left[\left|\uparrow^a\right\rangle\left(\left|\uparrow_x^P \uparrow_x^P\right\rangle - \left|\downarrow_x^P \downarrow_x^P\right\rangle\right) - \left|\downarrow^a\right\rangle\left(\left|\uparrow_x^P \uparrow_x^P\right\rangle + \left|\downarrow_x^P \downarrow_x^P\right\rangle\right)\right]$$

Subsequent measurement of the atomic state disentangles the atom, which results in a maximally entangled two-photon state: if the atom is found in $|\downarrow^a\rangle$ ($|\uparrow^a\rangle$), the resulting state is $\left|\Phi_{\mathrm{PP}}^+\right\rangle$ $\left(\left|\Phi_{\mathrm{PP}}^-\right\rangle\right)$, respectively. In

the experiment, the two-photon density matrices are again reconstructed with the maximum-likelihood technique (see Fig. 4 and Extended Data Table 1d and e). This gives a fidelity with the expected Bell states of 67(2)% (64(2)%) for the $\left|\Phi_{\mathrm{PP}}^+\right\rangle$ $\left(\left|\Phi_{\mathrm{PP}}^-\right\rangle\right)$ state. The values achieved prove photon–photon entanglement. Their small difference can be explained by the fact that a detection of the atom in $F = 1$ selects only those events where it has initially been prepared in the correct state $|\uparrow^a\rangle$, rather than in another state of the $F = 2$ hyperfine manifold. Again, we find a higher fidelity of maximally 76% with a rotated $\left|\Phi_{\mathrm{PP}}^+\right\rangle$ state with $\varphi = 0.25\pi$.

The above measurements demonstrate the versatility of the presented gate mechanism and its ability to mediate a photon–photon interaction. To this end, intermediate storage of the two photons during the time required to rotate and read out the atomic state (about 3 µs) is required, which can be implemented with an optical fibre less than one kilometre in length. Conditioned on the state of the atom, the polarization of the photons then has to be rotated using, for example, an electro-optical modulator. As an alternative to the eraser scheme used in this work, the first photon could be reflected from the cavity a second time[7].

In addition to the applications mentioned above[5–13], the gate mechanism we present here opens up perspectives for numerous quantum optics experiments. First, it could be applied to perform a quantum-non-demolition measurement of the polarization of a single reflected photon by measuring the state of the atom—conversely, it could be used to measure the atomic state without energy exchange[21] by measuring the polarization of a reflected photon. Second, a quantum gate between several atoms in the same or even in remote cavities[25,26] could be directly implemented, which would facilitate universal quantum computation in a decoherence-free subspace[27]. Last, the use of our gate mechanism in the proposed deterministic optical Bell-state measurement[12] would markedly increase the efficiency of teleportation between remote atoms[28,29], and would therefore improve the prospects for implementation of a quantum repeater[4] and a global-scale quantum network[3,30].
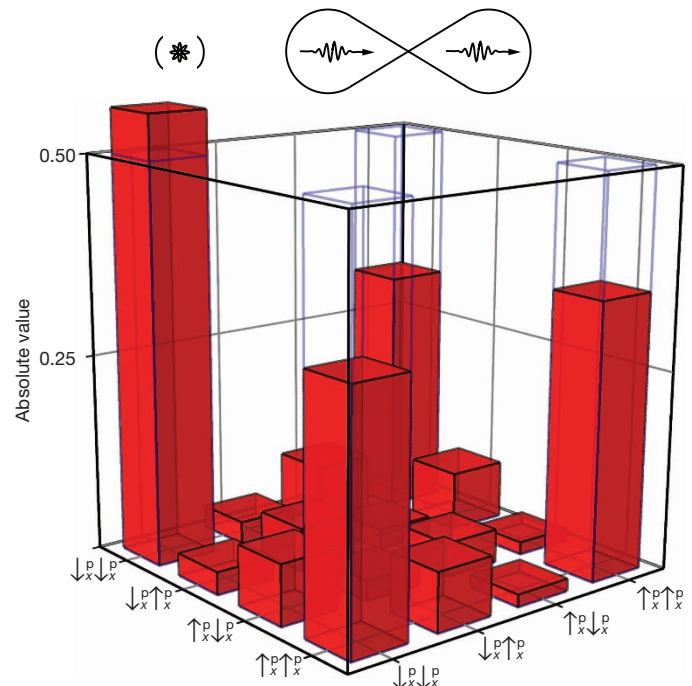

Figure 4 | Entangled photon–photon state generated via consecutive interaction with the atom. The bars show the absolute value of the density matrix elements. The fidelity with the maximally entangled $\left|\Phi_{\mathrm{PP}}^+\right\rangle$ Bell state (open blue bars) is 67(2)%. The diagram at the top of the figure symbolizes photon–photon entanglement.

METHODS SUMMARY

In the experimental set-up, single ^{87}Rb atoms are loaded from a magneto-optical trap into a three-dimensional optical lattice inside a Fabry–Perot cavity. The cavity is overcoupled, that is, the coupling mirror has a transmission (95 p.p.m.) which is large compared to the transmission of the other mirror in the cavity and the scattering and absorption losses (8 p.p.m. total). The geometry of the trap and the cooling mechanisms used are described in detail in ref. 16. The lattice consists of three retro-reflected laser beams, one red-detuned (1,064 nm) and two blue-detuned (770 nm) from the atomic transitions at 780 nm (D_2 line) and 795 nm (D_1 line). The use of high intensities leads to trap frequencies of several hundred kHz, which facilitates fast cooling to low temperatures using intra-cavity Sisyphus cooling. In each experimental cycle, a cooling interval of 0.8 ms is applied, which allows for atom trapping times of many seconds. In contrast to ref. 16, ground-state cooling is not applied in this work.

Online Content Any additional Methods, Extended Data display items and Source Data are available in the online version of the paper; references unique to these sections appear only in the online paper.

1. Gisin, N., Ribordy, G., Tittel, W. & Zbinden, H. Quantum cryptography. *Rev. Mod. Phys.* **74,** 145–195 (2002).
2. Ladd, T. D. *et al.* Quantum computers. *Nature* **464,** 45–53 (2010).
3. Duan, L.-M. & Monroe, C. Colloquium: Quantum networks with trapped ions. *Rev. Mod. Phys.* **82,** 1209–1224 (2010).
4. Briegel, H.-J., Dür, W., Cirac, J. I. & Zoller, P. Quantum repeaters: the role of imperfect local operations in quantum communication. *Phys. Rev. Lett.* **81,** 5932–5935 (1998).
5. Monroe, C. & Kim, J. Scaling the ion trap quantum processor. *Science* **339,** 1164–1169 (2013).
6. Awschalom, D. D., Bassett, L. C., Dzurak, A. S., Hu, E. L. & Petta, J. R. Quantum spintronics: engineering and manipulating atom-like spins in semiconductors. *Science* **339,** 1174–1179 (2013).
7. Duan, L.-M. & Kimble, H. J. Scalable photonic quantum computation through cavity-assisted interactions. *Phys. Rev. Lett.* **92,** 127902 (2004).
8. Reiserer, A., Ritter, S. & Rempe, G. Nondestructive detection of an optical photon. *Science* **342,** 1349–1351 (2013).
9. Cho, J. & Lee, H.-W. Generation of atomic cluster states through the cavity input-output process. *Phys. Rev. Lett.* **95,** 160501 (2005).
10. Hu, C. Y., Munro, W. J. & Rarity, J. G. Deterministic photon entangler using a charged quantum dot inside a microcavity. *Phys. Rev. B* **78,** 125318 (2008).
11. Wang, B. & Duan, L.-M. Engineering superpositions of coherent states in coherent optical pulses through cavity-assisted interaction. *Phys. Rev. A* **72,** 022320 (2005).
12. Bonato, C. *et al.* CNOT and Bell-state analysis in the weak-coupling cavity QED regime. *Phys. Rev. Lett.* **104,** 160503 (2010).
13. Munro, W. J., Stephens, A. M., Devitt, S. J., Harrison, K. A. & Nemoto, K. Quantum communication without the necessity of quantum memories. *Nature Photon.* **6,** 777–781 (2012).
14. Turchette, Q. A., Hood, C. J., Lange, W., Mabuchi, H. & Kimble, H. J. Measurement of conditional phase shifts for quantum logic. *Phys. Rev. Lett.* **75,** 4710–4713 (1995).
15. Fushman, I. *et al.* Controlled phase shifts with a single quantum dot. *Science* **320,** 769–772 (2008).
16. Reiserer, A., Nölleke, C., Ritter, S. & Rempe, G. Ground-state cooling of a single atom at the center of an optical cavity. *Phys. Rev. Lett.* **110,** 223003 (2013).
17. Paris, M. & Řeháček, J. *Quantum State Estimation* (Springer, 2004).
18. Duan, L.-M. & Raussendorf, R. Efficient quantum computation with probabilistic quantum gates. *Phys. Rev. Lett.* **95,** 080503 (2005).
19. van Enk, S. J., Cirac, J. I. & Zoller, P. Photonic channels for quantum communication. *Science* **279,** 205–208 (1998).
20. Dayan, B. *et al.* A photon turnstile dynamically regulated by one atom. *Science* **319,** 1062–1065 (2008).
21. Volz, J., Gehr, R., Dubois, G., Estéve, J. & Reichel, J. Measurement of the internal state of a single atom without energy exchange. *Nature* **475,** 210–213 (2011).
22. Thompson, J. D. *et al.* Coupling a single trapped atom to a nanoscale optical cavity. *Science* **340,** 1202–1205 (2013).
23. O'Shea, D., Junge, C., Volz, J. & Rauschenbeutel, A. Fiber-optical switch controlled by a single atom. *Phys. Rev. Lett.* **111,** 193601 (2013).
24. Rauschenbeutel, A. *et al.* Step-by-step engineered multiparticle entanglement. *Science* **288,** 2024–2028 (2000).
25. Xiao, Y.-F. *et al.* Realizing quantum controlled phase flip through cavity QED. *Phys. Rev. A* **70,** 042314 (2004).
26. Duan, L.-M., Wang, B. & Kimble, H. J. Robust quantum gates on neutral atoms with cavity-assisted photon scattering. *Phys. Rev. A* **72,** 032333 (2005).
27. Xue, P. & Xiao, Y.-F. Universal quantum computation in decoherence-free subspace with neutral atoms. *Phys. Rev. Lett.* **97,** 140501 (2006).
28. Olmschenk, S. *et al.* Quantum teleportation between distant matter qubits. *Science* **323,** 486–489 (2009).
29. Nölleke, C. *et al.* Efficient teleportation between remote single-atom quantum memories. *Phys. Rev. Lett.* **110,** 140403 (2013).
30. Ritter, S. *et al.* An elementary quantum network of single atoms in optical cavities. *Nature* **484,** 195–200 (2012).

METHODS

Experimental set-up. In the experimental set-up, single ^{87}Rb atoms are loaded from a magneto-optical trap into a three-dimensional optical lattice inside a Fabry–Perot cavity. The cavity is overcoupled, that is, the coupling mirror has a transmission (95 p.p.m.) which is large compared to the transmission of the other mirror in the cavity and the scattering and absorption losses (8 p.p.m. total). The geometry of the trap and the employed cooling mechanisms are described in detail in ref. 16. The lattice consists of three retro-reflected laser beams, one red-detuned (1,064 nm) and two blue-detuned (770 nm) from the atomic transitions at 780 nm (D$_2$ line) and 795 nm (D$_1$ line). The use of high intensities leads to trap frequencies of several hundred kHz, which facilitates fast cooling to low temperatures using intra-cavity Sisyphus cooling. In each experimental cycle, a cooling interval of 0.8 ms is applied, which allows for atom trapping times of many seconds. In contrast to ref. 16, ground-state cooling is not applied in this work.

Light shift. For the working principle of the gate, the a.c. Stark shift of the atomic levels is important, which is schematically depicted in Fig. 1a. In this context, the blue-detuned trap light has a negligible influence, because the atom is trapped at a node of the standing-wave light field. The red-detuned light, however, considerably shifts the frequency of the atomic transitions, depending on the polarization of the trap laser. We employ π-polarized light, that is, the electric field vector is oriented parallel to the quantization axis, which coincides with the cavity axis and the direction of an externally applied magnetic field of about 0.5 G. In this configuration, the a.c. Stark shift is identical for all Zeeman states in the ground-state manifolds with $F = 1$ and $F = 2$. The excited state $F' = 3$, however, experiences a Zeeman-state-dependent shift. Its value has been measured for the atomic transition $|2, 2\rangle \leftrightarrow |3, 3\rangle$ to be 0.10 GHz, where 0.05 GHz stems from the shift of the ground state $|2, 2\rangle$. The shifts of the other states in the $F' = 3$ manifold can be calculated by summing over all relevant atomic levels considering the individual transition strengths. This leads to the following level shifts: $|3, 0\rangle$, 0.16 GHz; $|3, \pm1\rangle$, 0.15 GHz; $|3, \pm2\rangle$, 0.10 GHz; $|3, \pm3\rangle$, 0.05 GHz.

In the context of the gate mechanism, the impinging photon is on resonance with the transition $|2, 2\rangle \leftrightarrow |3, 3\rangle$. The transition $|2, 2\rangle \leftrightarrow |3, 1\rangle$ is thus detuned by 0.1 GHz, while all transitions from the $F = 1$ state are detuned by about 7 GHz. Therefore, only the atom in state $|\uparrow^a\rangle$ and the photon in $|\uparrow^P\rangle$ are strongly coupled.

Atomic state preparation. To prepare the atom in the state $|2, 2\rangle$, a 140-μs-long interval of optical pumping is used, where circularly polarized light is applied on resonance along the cavity axis and an additional repumping laser depletes the states with $F = 1$. Once the atom is pumped to the desired state, the transmission of the pump light is strongly reduced owing to strong coupling. Monitoring the cavity output with single-photon counting modules thus allows us to preselect those experimental runs in which the atom has been pumped to the right state with high probability[8]. The experimental results presented in this work were obtained by selecting those cases where one or zero photons were detected in the last 10 μs of the optical pumping interval, which is about half of all attempts.

Atomic state detection. To detect the atomic hyperfine state, cavity-enhanced fluorescence state detection is employed. To this end, a laser resonant with the cavity is applied from the side[16]. If the atom is in the state $F = 2$, it scatters many photons into the cavity (enhanced by the Purcell effect), whereas there is no scattering if the atom is in the state $F = 1$ owing to the large atom–laser detuning of 7 GHz. The described technique only detects the hyperfine state and is not sensitive to the atomic Zeeman state. Compared to previous experiments[8], the time required to detect the atomic state could be reduced from 25 μs to 3 μs by increasing the power of the applied laser beam. Further reduction is possible, but at the price of a reduced atom-trapping time. A histogram of the detected photon number per run is depicted in Extended Data Fig. 1. When the atom is prepared in a state with $F = 1$ (red), no photons are detected in 99.7% of all cases. When the atom is prepared in $|2, 2\rangle$ (blue), one or more photons are detected in 99.6% of the runs. Thus, when setting the threshold between 0 and 1 detected photons, the state detection fidelity is 99.65%.

Atomic state rotation. In order to rotate the atomic state, we employ a pair of co-propagating Raman laser beams with orthogonal polarization, applied from the side of the cavity with a detuning of −0.15 THz from the D$_1$ line. A magnetic field applied along the cavity axis splits the atomic Zeeman states by 0.3 MHz, which allows us to spectrally address individual transitions. To investigate the quality of the combined atomic-state preparation, rotation and readout process, Ramsey spectroscopy is performed. To this end, the atom is prepared in the state $|2, 2\rangle$ and two π/2 Raman pulses are applied (duration, 1.7 μs; temporal separation, 7.5 μs). The result of a subsequent measurement of the atomic state is shown in Extended Data Fig. 2. At zero detuning, this sequence would ideally result in a transfer probability of 100% when the two pulses are applied with the same phase (black). Experimentally, we observe 95(1)%. Scanning the laser frequency over a few tens of kHz, a sinusoidal oscillation is observed, which, as expected, shifts by a quarter of a period when the second Ramsey pulse is applied with a phase difference of π/2 (red). From the difference between the maximum and minimum values of the observed curve, 90(2)%, we conclude that the atomic state preparation, rotation and readout process works as intended in 95(1)% of the experiments, which includes dephasing during the 7.5 μs between the Raman pulses.

Experimental imperfections. In this section, the major experimental imperfections that reduce the fidelity of the atom–photon entangled state (Fig. 2) with $\left|\Phi_{\text{ap}}^+\right\rangle$ are explained in more detail. As the effects are expected to be uncorrelated, they are considered independently.

The major contribution stems from the spatial mismatch between the Gaussian cavity mode and the transversal mode profile of the impinging photons. The mismatch is independently measured to be $\xi = 8(3)\%$. The unmatched fraction of the pulse will be reflected from the cavity without a phase shift, leaving both the atom and the photon in their initial state. This product state has a fidelity of $F_u = 0.25$ with the desired Bell state. The matched fraction, however, is only reflected in $\varepsilon = 69\%$ of the cases. This leads to an estimated reduction of the fidelity of

$$\frac{\xi}{\xi + (1 - \xi)\varepsilon} \times (1 - F_u) = 8(3)\%$$

The quality of our atomic state preparation, rotation and readout also limits the achievable fidelity. In the Ramsey spectroscopy measurement (see Extended Data Fig. 2), we detect the atom in the expected state with a probability of 95(1)%. We therefore expect a fidelity reduction of 5(1)%.

Besides, imperfections in the photonic polarization measurement arise from two effects: from detector dark counts (3.3% of all detection events) and from the polarizing beam splitters used in the experiment (extinction ratio about 100:1 in reflection, 1,000:1 in transmission). The combined fidelity reduction of both effects is $(1 - F_u) \times 3.3\% + 0.5\% \approx 3\%$.

Finally, the gate is characterized with faint laser pulses that have a mean photon number of $\bar{n} = 0.07$. The evaluation is conditioned on the detection of a single photon. Owing to the Poissonian photon number statistics, 4% of these single-photon detection events are caused by higher photon-number contributions in the input. This value is calculated[8] by considering the measured absorption of the set-up and the quantum efficiency ($\eta = 0.6$) of the single-photon counters. In about half of the two-photon cases, both photons were reflected (generating a GHZ state as explained in the main text) but only one was detected. Then, the detected atom–photon state would be classically correlated with $F_c = 0.5$, giving a total reduction of the entanglement fidelity of $F_c \times 2\% = 1\%$. In the other half of the cases, one of the two photons was absorbed. Thus, the atomic quantum state is partially projected: while the uncoupled $|\downarrow^P\rangle$ polarization component would leave the atom in the initial state, the coupled $|\uparrow^P\rangle$ component would fully project the atomic state. Therefore, the resulting fidelity reduction for an absorbed photon is $(1 - F_u) \times 0.5 \times 2\% \approx 1\%$. The overall fidelity reduction due to two-photon components is thus 2%.
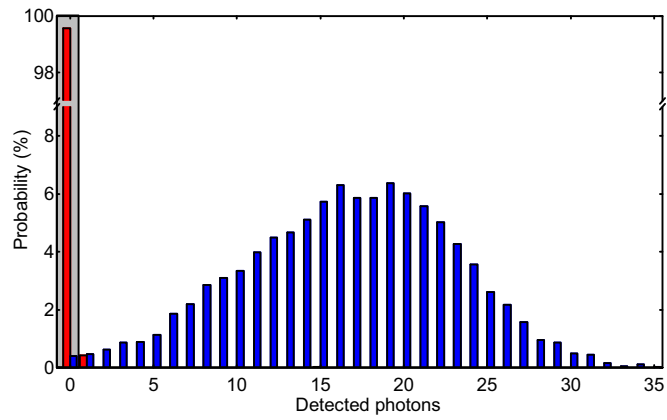
Extended Data Figure 1 | Detection of the atomic state. The atom is prepared either in the resonant $|2, 2\rangle$ state (blue) or in the detuned $F = 1$ state (red) and a resonant laser is applied for 3 μs from the side of the cavity. The number of photons detected in the cavity output allows us to distinguish the two cases with a fidelity of 99.65%.
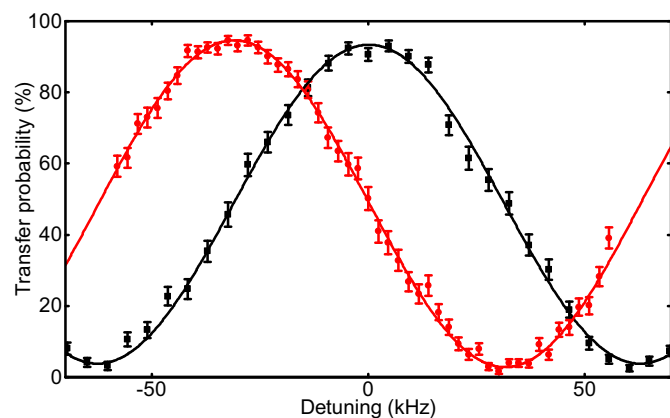
Extended Data Figure 2 | Ramsey spectroscopy. The atom is prepared in the state $|2, 2\rangle$ and two $\pi/2$ Raman pulses are applied with a temporal separation of 7.5 μs. As the Raman laser detuning is scanned, a sinusoidal oscillation is observed. The error bars denote the s.e.m. When the second pulse is applied with a phase shift of $\pi/2$ (red), the curve is shifted by a quarter of a period with respect to the case without phase shift (black). From the amplitude of the sinusoidal fit curves, we deduce that the atomic state preparation, rotation and readout works as intended in 95(1)% of the experiments.

Extended Data Table 1 | Numerical values of the truth table and density matrices

a

	$\downarrow^a\downarrow^p_x$	$\downarrow^a\uparrow^p_x$	$\uparrow^a\downarrow^p_x$	$\uparrow^a\uparrow^p_x$
$\downarrow^a\downarrow^p_x$	0.989	0.008	0.003	0.000
$\downarrow^a\uparrow^p_x$	0.010	0.987	0.000	0.003
$\uparrow^a\downarrow^p_x$	0.002	0.005	0.139	0.855
$\uparrow^a\uparrow^p_x$	0.003	0.001	0.870	0.126

b

	$\downarrow^a\downarrow^p_x$	$\downarrow^a\uparrow^p_x$	$\uparrow^a\downarrow^p_x$	$\uparrow^a\uparrow^p_x$
$\downarrow^a\downarrow^p_x$	0.510	h.c.	h.c.	h.c.
$\downarrow^a\uparrow^p_x$	0.059 - 0.020 i	0.016	h.c.	h.c.
$\uparrow^a\downarrow^p_x$	- 0.039 - 0.002 i	- 0.005 - 0.019 i	0.077	h.c.
$\uparrow^a\uparrow^p_x$	0.353 - 0.131 i	0.026 - 0.010 i	- 0.011 + 0.017 i	0.398

c

	$\downarrow^a\downarrow^p_x\downarrow^p_x$	$\downarrow^a\downarrow^p_x\uparrow^p_x$	$\downarrow^a\uparrow^p_x\downarrow^p_x$	$\downarrow^a\uparrow^p_x\uparrow^p_x$	$\uparrow^a\downarrow^p_x\downarrow^p_x$	$\uparrow^a\downarrow^p_x\uparrow^p_x$	$\uparrow^a\uparrow^p_x\downarrow^p_x$	$\uparrow^a\uparrow^p_x\uparrow^p_x$
$\downarrow^a\downarrow^p_x\downarrow^p_x$	0.494	h.c.	h.c.	h.c.	h.c.	h.c.	h.c.	h.c.
$\downarrow^a\downarrow^p_x\uparrow^p_x$	0.053 - 0.004 i	0.021	h.c.	h.c.	h.c.	h.c.	h.c.	h.c.
$\downarrow^a\uparrow^p_x\downarrow^p_x$	0.054 - 0.015 i	0.013 + 0.008 i	0.025	h.c.	h.c.	h.c.	h.c.	h.c.
$\downarrow^a\uparrow^p_x\uparrow^p_x$	- 0.007 - 0.027 i	- 0.001 + 0.001 i	0.003 - 0.006 i	0.009	h.c.	h.c.	h.c.	h.c.
$\uparrow^a\downarrow^p_x\downarrow^p_x$	0.006 + 0.012 i	0.013 - 0.003 i	0.007 - 0.007 i	- 0.007 + 0.001 i	0.028	h.c.	h.c.	h.c.
$\uparrow^a\downarrow^p_x\uparrow^p_x$	0.020 - 0.022 i	0.010 - 0.005 i	0.021 + 0.001 i	- 0.007 + 0.006 i	0.010 + 0.002 i	0.054	h.c.	h.c.
$\uparrow^a\uparrow^p_x\downarrow^p_x$	0.060 - 0.035 i	0.004 + 0.001 i	+ 0.012 + 0.002 i	- 0.002 + 0.004 i	- 0.020 + 0.008 i	0.023 - 0.009 i	0.057	h.c.
$\uparrow^a\uparrow^p_x\uparrow^p_x$	- 0.212 + 0.163 i	- 0.028 + 0.030 i	- 0.006 + 0.040 i	- 0.004 + 0.010 i	- 0.005 - 0.008 i	0.017 + 0.019 i	- 0.029 + 0.025 i	0.311

d

	$\downarrow^p_x\downarrow^p_x$	$\downarrow^p_x\uparrow^p_x$	$\uparrow^p_x\downarrow^p_x$	$\uparrow^p_x\uparrow^p_x$
$\downarrow^p_x\downarrow^p_x$	0.556	h.c.	h.c.	h.c.
$\downarrow^p_x\uparrow^p_x$	0.013 + 0.025 i	0.054	h.c.	h.c.
$\uparrow^p_x\downarrow^p_x$	- 0.076 - 0.003 i	0.024 + 0.008 i	0.042	h.c.
$\uparrow^p_x\uparrow^p_x$	0.218 - 0.222 i	0.074 - 0.004 i	0.016 - 0.001 i	0.348

e

	$\downarrow^p_x\downarrow^p_x$	$\downarrow^p_x\uparrow^p_x$	$\uparrow^p_x\downarrow^p_x$	$\uparrow^p_x\uparrow^p_x$
$\downarrow^p_x\downarrow^p_x$	0.538	h.c.	h.c.	h.c.
$\downarrow^p_x\uparrow^p_x$	0.112 - 0.020 i	0.087	h.c.	h.c.
$\uparrow^p_x\downarrow^p_x$	0.066 - 0.045 i	0.068 + 0.003 i	0.073	h.c.
$\uparrow^p_x\uparrow^p_x$	- 0.223 + 0.044 i	- 0.009 + 0.045 i	- 0.016 + 0.059 i	0.303

a, Data of the truth table measurement depicted in Fig. 1. **b**, Atom–photon density matrix. The absolute values of the elements are depicted in Fig. 2. **c**, Atom–photon–photon density matrix. The absolute values of the elements are depicted in Fig. 3. **d**, Photon–photon density matrix, post-selected on the detection of the atomic $|\downarrow^a\rangle$ state. The absolute values of the elements are depicted in Fig. 4. **e**, Photon–photon density matrix, post-selected on the detection of the atomic $|\uparrow^a\rangle$ state. h.c., Hermitian conjugate.